Volume 17
Number 1
January 2026
Pages 1–726

RSC Medicinal Chemistry

rsc.li/medchem

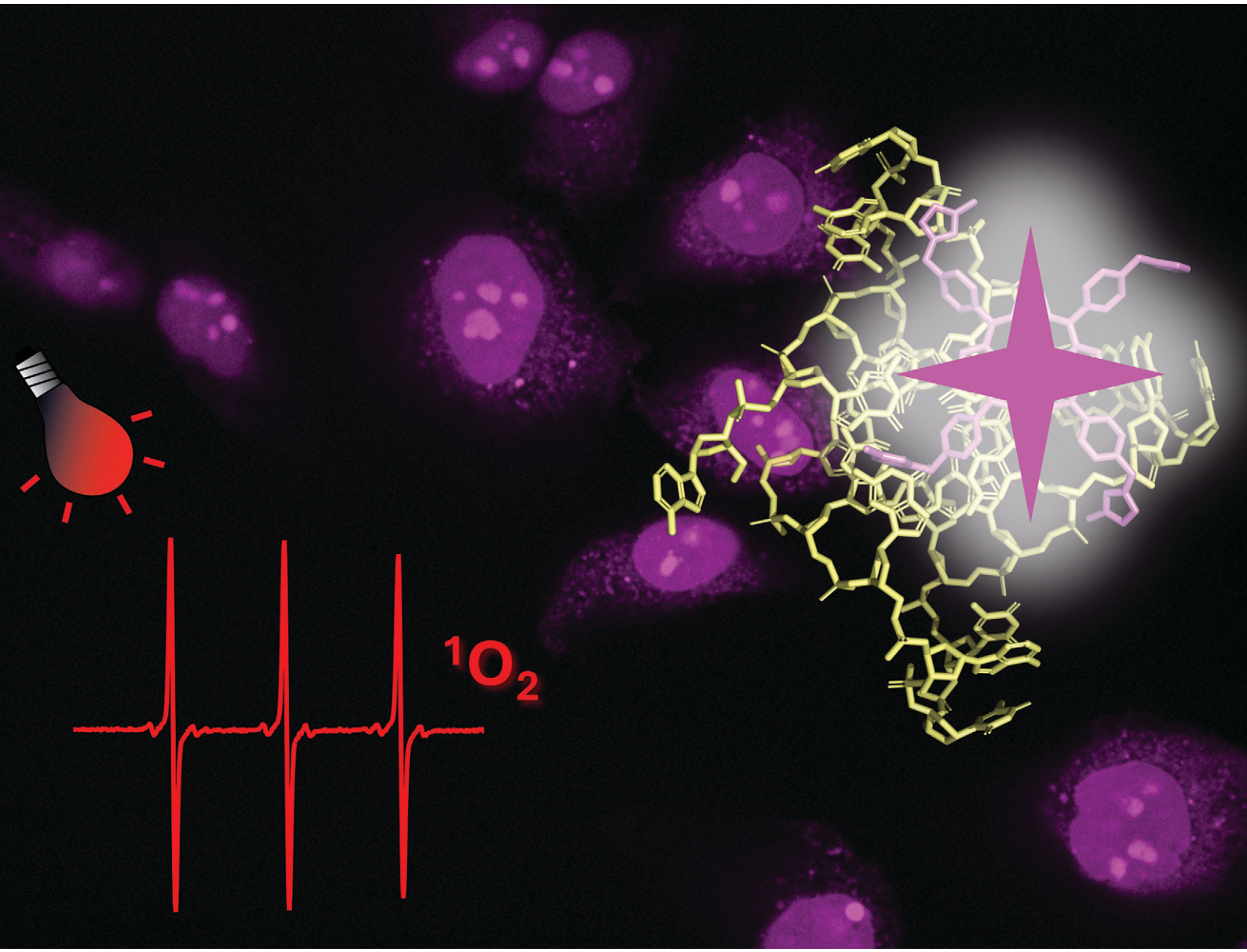

ISSN 2632-8682

ROYAL SOCIETY OF CHEMISTRY

RESEARCH ARTICLE

Naoko Yoshizawa-Sugata, Hisao Masai, Yoko Yamakoshi *et al.*
Water-soluble cationic porphyrins with enhanced phototoxicity to cancer cell lines for G4-targeting photodynamic therapy

RSC Medicinal Chemistry

ROYAL SOCIETY OF CHEMISTRY

RESEARCH ARTICLE

View Article Online
View Journal | View Issue

Check for updates

Cite this: *RSC Med. Chem.*, 2026, **17**, 225

Water-soluble cationic porphyrins with enhanced phototoxicity to cancer cell lines for G4-targeting photodynamic therapy

Çetin Çelik, [a] Naoko Kakusho, [b] Tianyu Xu, [a] Sung Sik Lee, [c] Naoko Yoshizawa-Sugata, *[d] Hisao Masai *[b] and Yoko Yamakoshi *[a]

Received 8th August 2025,
Accepted 30th September 2025

DOI: 10.1039/d5md00706b

rsc.li/medchem

Porphyrins are well-known photosensitizers (PSs), a few of which are clinically approved drugs for use in photodynamic therapy (PDT). Porphyrin derivatives including tetra-cationic porphyrins, *e.g.* **TMPyP4**, are also well-studied binders for G-quadruplex (G4) DNA. Since G4 DNAs are known to play a role in malignant transformation of cells, a variety of G4 binders have been used in cancer therapy by regulating the function of G4 DNA. In this study, two water-soluble porphyrins (**1** and **2**), with four terminal cationic moieties connected with alkyl linkers were synthesized as bifunctional molecules for simultaneous G4 binding and PDT-PS. Photoinduced singlet oxygen ($^1O_2$) generation and DNA cleavage were tested under visible light irradiation revealing the efficient generation of $^1O_2$ in line with photoinduced DNA cleavages. Studies in a cancer cell line (HeLa) and a normal fibroblast (NHDF) cells revealed significantly stronger photocytotoxicities of these porphyrins (**1** and **2**) in comparison to **TMPyP4**, presumably due to better cellular internalization – as observed by flow cytometry. Interestingly, enhanced photocytotoxicity of **1** and **2** was observed in HeLa in comparison to NHDF. This may be related to the fact that more G4 DNAs are present in the nuclei of cancer cell lines to allow binding of porphyrins **1** and **2**, as observed by fluorescence microscopy. The interactions of porphyrins **1** or **2** with a G4-forming telomeric DNA were evaluated by a FRET assay and spectroscopic methods (fluorescence, UV-vis, and CD) and showed selective binding to G4 DNA. The results show the potential of porphyrins **1** and **2** as PDT-PSs targeting cancer cells with higher G4-forming domains.

Open Access Article. Published on 01 October 2025. Downloaded on 6/13/2026 9:49:03 PM.
This article is licensed under a Creative Commons Attribution-NonCommercial 3.0 Unported Licence.

Introduction

Photodynamic therapy (PDT) is a non-surgical treatment used for various types of cancers by the function of reactive oxygen species (ROS) generated by photosensitizers (PSs) under photoirradiation. Most PDT-PS drugs approved or in clinical trials are porphyrin derivatives.[1,2] In addition to their excellent ability to generate ROSs under visible light irradiation, several *in vivo* and *in vitro* studies report that porphyrins localize more in cancer cells compared to healthy cells.[3–7] This indicates their potential as PDT-PSs, enhancing damage to cancer cells while reducing unwanted damage to healthy cells.[8] However, many porphyrins suffer from low solubility in biological media, often requiring the addition of solubilizing groups or polar substituents. Furthermore, to improve cellular uptake,[9] amphiphilic types of porphyrins would be advantageous due to their sufficient water-solubility and lipophilicity.

Porphyrin derivatives are also known binders for guanine-quadruplex (G4), one of the higher-order structures of DNA often found in guanine-rich domains. Typically, in the presence of cations such as K^+ and Na^+, four guanine moieties form a tetrad structure *via* the Hoogsteen-type hydrogen bonds to further form assemblies by stacking. G4 binders have attracted attention in relation to cancers and other biological functions.[10–15] For instance, promoters of oncogenes, often (>40%) containing at least one G4 motif,[16] can be stabilized by G4 binders to downregulate corresponding oncogenes.[17] G4 motifs are also found in the human telomeric repeat (TTAGGG), where G4 binders stabilize their 3-D structures to disrupt the capping function of telomerases,[18,19] which are expressed more in cancer cells.[20,21] For these reasons, many researchers have worked on developing stronger and more selective G4-binding and/or G4-stabilizing

[a] *Department of Chemistry and Applied Biosciences, ETH Zürich, Vladimir-Prelog-Weg 3, CH-8093 Zürich, Switzerland. E-mail: yamakoshi@org.chem.ethz.ch*
[b] *Department of Basic Medical Sciences, Tokyo Metropolitan Institute of Medical Science, 2-1-6 Kamikitazawa, Setagaya, Tokyo 156-8506, Japan. E-mail: masai-hs@igakuken.or.jp*
[c] *ScopeM, ETH Zürich, Otto-Stern-Weg 3, CH-8093 Zürich, Switzerland*
[d] *Research Center for Genome & Medical Sciences, Tokyo Metropolitan Institute of Medical Science, 2-1-6 Kamikitazawa, Setagaya, Tokyo 156-8506, Japan. E-mail: yoshizawa-nk@igakuken.or.jp*

Open Access Article. Published on 01 October 2025. Downloaded on 6/13/2026 9:49:03 PM. This article is licensed under a Creative Commons Attribution-NonCommercial 3.0 Unported Licence.

molecules.[11] These molecules will help not only to understand the fundamental biological function of G4, but will also be useful as therapeutic drugs for selective cancer treatments.[22,23]

Among many G4-binding small molecules,[24] a tetra-cationic porphyrin, **TMPyP4** (Fig. 1), having a planar core with four cationic moieties at its edge, has been known as a standard molecule that interacts with negatively charged phosphate backbones in G4 structures.[25] Considering the aforementioned photoinduced ROS generation by porphyrins, **TMPyP4** and related compounds were reported as a potential core for G4-targeted PSs for photodynamic therapy (PDT).[26–33] However, despite of its binding ability to G4 DNAs, **TMPyP4** suffers from relatively low binding selectivity to G4 DNA over double strand DNA (dsDNA)[34,35] and limited cellular accumulation.[36]

In this study, we synthesized two water-soluble cationic porphyrins **1** and **2** with an extended distance of cations from the porphyrin centre (Fig. 1). Distinct from **TMPyP4**, compounds **1** and **2** possess cationic moieties through short anchors at the edges of the porphyrin core to enhance the distance from the centre, as indicated in the electrostatic surface potential map (lower row of Fig. 1 and S1). We expected that the flexible cation location in **1** and **2** could potentially allow a better alignment of the ligand with respect to the negatively charged phosphate backbone of DNA.[37] These cationic moieties, guanidinium[38–40] and 1-methyl imidazolium,[41] were reported to interact with phosphate in G4 DNA. Furthermore, porphyrins **1** and **2** with higher amphiphilicities than **TMPyP4** may reveal better cellular uptake. Based on the assumptions above, porphyrins **1** and **2** were designed and synthesized.[42,43] Photoinduced singlet oxygen ($^1O_2$) generation, DNA-cleaving activity, and cytotoxicity were studied to evaluate them as PDT-PS molecules, together with cellular uptake, G4-stabilizing and binding abilities.

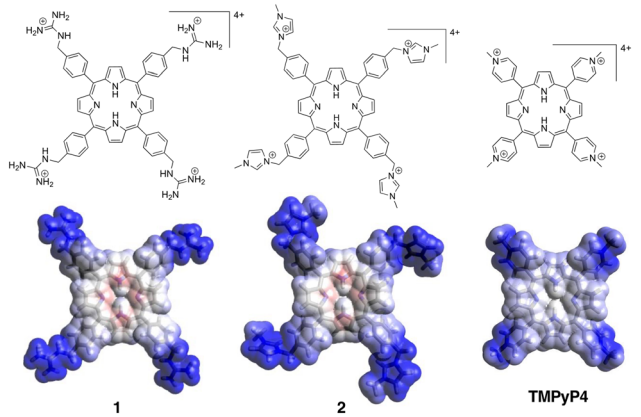

Fig. 1 Chemical structures and electrostatic surface potential maps for porphyrin **1**, porphyrin **2**, and **TMPyP4**. Conformation optimization and electrostatic surface potential calculation were performed using the universal force field operated with Avogadro 1.2.0. Blue: lower electron density; red: higher electron density.

Results and discussion

Syntheses of compounds 1 and 2

Porphyrins **1** and **2** were synthesized *via* the Lindsey method[44] from the corresponding aldehydes and pyrrole (Schemes S1 and S2). For **1**, cleavage of the phthalimide groups of **S3** gave a porphyrin amine derivative **S4**, which was subjected to guanidinylation to provide **1**. For **2**, a bromo substituted porphyrin **S5** was converted to porphyrin **2** by the reaction with 1-methylimidazole (Scheme S2).[43] Both compounds **1** and **2** were purified by reverse phase HPLC (Fig. S10 and S22) and structures were confirmed by ^1H and ^{13}C NMR and HRMS (Fig. S11–S16 and S23–S28).

Fig. 2a shows the UV-vis spectra of porphyrins **1** and **2** and the control G4 binder **TMPyP4**. The characteristic spectra for metal-free porphyrins with a Soret band at around 420 nm and four Q bands at *ca.* 500–650 nm were observed in all porphyrins. Fluorescence spectra (Fig. 2b) were acquired using an excitation wavelength of 420 nm and revealed that porphyrins **1** and **2** were highly fluorescent in comparison to **TMPyP4**. There was no aggregation observed in porphyrins **1**, **2** and **TMPyP4** in pH 7.4 HEPES buffer at least 10 μM as indicated by linear correlation of absorption intensity *versus* concentration at the Soret band (Fig. S18 and S30). The

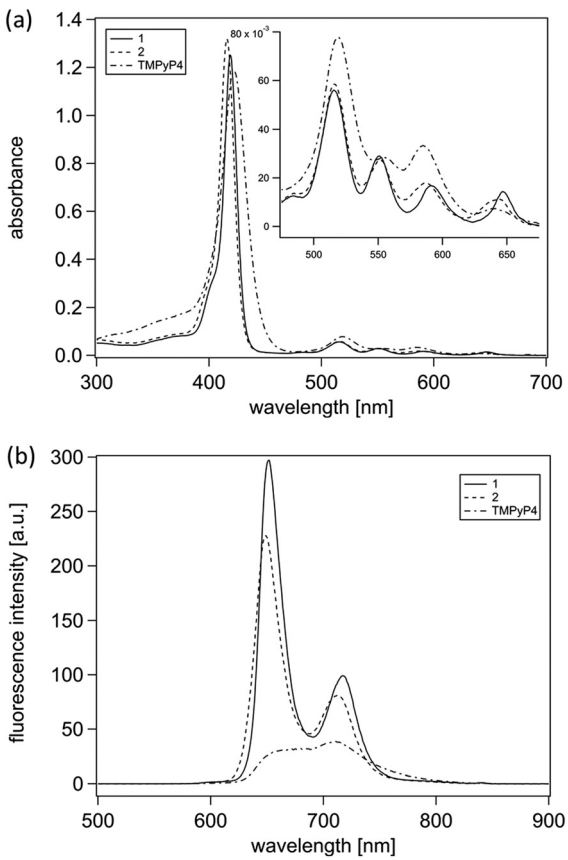

Fig. 2 UV-vis (a) and fluorescence (b) spectra of porphyrins **1**, **2**, and **TMPyP4** (5 μM in 10 mM HEPES buffer (pH 7.4)). Fluorescence spectra were recorded with an excitation wavelength at 420 nm using a slit of 5 nm.

This journal is © The Royal Society of Chemistry 2026

Open Access Article. Published on 01 October 2025. Downloaded on 6/13/2026 9:49:03 PM. This article is licensed under a Creative Commons Attribution-NonCommercial 3.0 Unported Licence.

higher fluorescence intensity of porphyrins **1** and **2** may be related to their larger hydrophobic core in comparison to **TMPyP4** leading to less quenching by water molecules.[45] There was no detectable aggregation of the molecules by DLS measurements at least up to 1 mM.

Photoinduced singlet oxygen generation and dsDNA cleavage

Photosensitivities of **1**, **2**, and **TMPyP4** were evaluated by singlet oxygen ($^1O_2$) generation under visible light irradiation. An ESR spin trapping method was employed for the detection of $^1O_2$ using 4-oxo-TEMP as a spin-trapping agent (scheme in Fig. 3).[46] Upon irradiation with green LEDs (539–541 nm), specific peaks corresponding to 4-oxo-TEMPO ($^1O_2$ adduct of 4-oxo-TEMP) were observed in the solution of each porphyrin (Fig. 3) in an irradiation-time-dependent manner (Fig. S32–S37), confirming that the type II energy transfer pathway was occurring due to porphyrins **1** and **2**. The relative amount of generated $^1O_2$ by each porphyrin was evaluated using the double integration value of ESR spectra (Fig. S38). By taking into account the relative absorption intensity of each porphyrin at 540 nm, the ability of $^1O_2$ generation by porphyrins **1** and **2** under photoirradiation (540 nm) for 2 or 10 min was respectively *ca.* 1.4–2.0 and 1.1–1.4 times higher, which was enhanced more at 621 nm, which is advantageous in the PDT application due to the better tissue penetration of light.

Alternatively, we also tried to observe type I ROS ($O_2^{\bullet-}$) generated by the electron transfer mechanism. Under visible light irradiation, generation of $O_2^{\bullet-}$ was clearly observed as an adduct of a spin-trapping agent, DEPMPO (Fig. S39 in the SI). However, the signals corresponding to DEPMPO·OOH were significantly suppressed in the presence of L-histidine (a $^1O_2$ quencher), suggesting that observed $O_2^{\bullet-}$ was generated not by type I but by the reduction of $^1O_2$ once generated *via* the type II pathway.

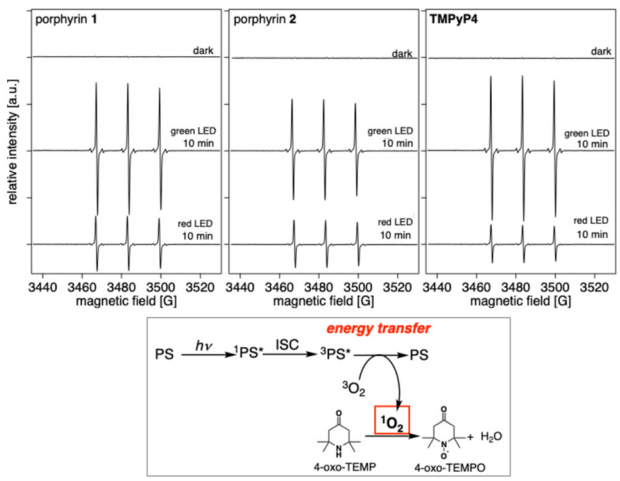

Fig. 3 X band ESR spectra of the $^1O_2$ adduct of 4-oxo-TEMP observed under irradiation of visible light (green LED: 539–541 nm, 90 ± 34% lm W^{-1}; red LED: 616–626 nm, 30 ± 37% lm W^{-1}) for 10 min. Conditions: porphyrin: 50 μM; 4-oxo-TEMP: 80 mM in pH 7.4 PBS(–).

As we observed sufficient $^1O_2$ generation by these porphyrins under visible light (green and red), we then tested their photoinduced damage to biomolecules (*e.g.* DNA). Such photoinduced DNA cleavage tests are often used as an initial assay to evaluate the photosensitivity of molecules for their potential as PDT-PS drugs. Using the pBR322 supercoiled DNA as a substrate dsDNA, DNA photo-cleavage tests were carried out by co-incubation with each porphyrin at various concentrations under visible light irradiation (527 nm green LED, 90 ± 34% lm W^{-1} or 630 nm red LED, 30 ± 37% lm W^{-1}) and subsequent gel electrophoresis analyses.

As shown in Fig. 4a, under light irradiation, DNA cleavage was observed for all porphyrins in a dose-dependent manner. Under green LED irradiation, DNA cleavage was observed in a similar range of concentrations for all porphyrins (**2** = **TMPyP4** > **1**, Fig. 4b), while both **1** and **2** showed enhanced DNA cleavage activity compared to **TMPyP4** under red light (**2** > **1** ≫ **TMPyP4**, Fig. 4c). In the presence of histidine, DNA cleavages by all three porphyrins were strongly reduced indicating that $^1O_2$ plays an important role in the DNA cleavage by these porphyrins (Fig. S41). This result was in line with the parallel data for higher $^1O_2$ generation and stronger DNA cleavage observed in porphyrins **1** and **2** in comparison to **TMPyP4**, confirming the essential role of $^1O_2$ in the photoinduced DNA cleavage by these porphyrins.

Photocytotoxicity

Following the significant $^1O_2$ generation and photoinduced DNA cleavage above, the porphyrins **1** and **2** were evaluated

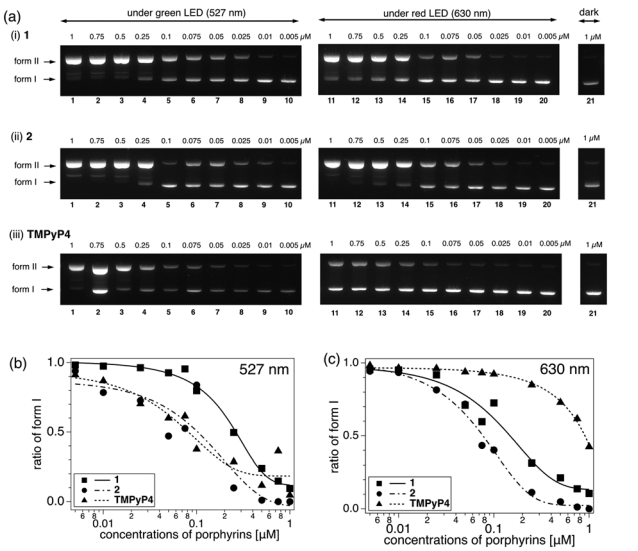

Fig. 4 (a) Photoinduced DNA cleavage of pBR322 DNA by **1**, **2** and **TMPyP4** under irradiation with LED light with a maximum at 527 nm (green, lanes 1–10) or at 630 nm (red, lanes 11–20) for 10 min. DNA: 12.5 μg mL^{-1} in Tris–HCl-EDTA buffer (pH 8.0). (b and c) Ratio of form I intact DNA after photoirradiation (b: 527 nm, 230 mW cm^{-2}; c: 630 nm, 255 mW cm^{-2}) in the presence of various concentrations of **1**, **2**, and **TMPyP4**, quantified using ImageJ.

Open Access Article. Published on 01 October 2025. Downloaded on 6/13/2026 9:49:03 PM. This article is licensed under a Creative Commons Attribution-NonCommercial 3.0 Unported Licence.

by photocytotoxicity tests. A cancer cell line (HeLa) and normal cells (NHDF) were used for the assays. Based on the standard methods,[47] cells were co-incubated with porphyrins at various concentrations for 24 h and then washed with PBS(−). There was no significant aggregation observed in the porphyrin solutions in medium after 24 h (Fig. S42). In the preliminary test, cellular uptake of the porphyrins was saturated at least after incubation for 24 h (Fig. S43). Subsequently, the cells were exposed to light irradiation with green (527 nm, 230 mW cm^{-2}) or red (630 nm, 255 mW cm^{-2}) LEDs and subjected to an MTT assay for viability after 3 h of incubation.

Under dark conditions, all porphyrins (**1**, **2**, and **TMPyP4**) showed no specific cytotoxicity up to at least 10 μM (Fig. 5) on either cell line. In contrast, under photoirradiation conditions, cell viability was significantly decreased in the presence of the porphyrins dose-dependently on both cell lines. Interestingly, porphyrins **1** and **2** showed much higher photocytotoxicity in comparison to the control **TMPyP4**, under the irradiation of both green and red lights (Fig. 5), despite their similar $^1O_2$ generation (Fig. 3) and DNA-cleaving activity (Fig. 4).

Importantly, porphyrins **1** and **2** showed significantly higher photocytotoxicity on a cancer cell line (HeLa) than on normal cells (NHDF) especially under the irradiation of red light (Fig. 5a and b in the right column and Table 1). This interesting phenomenon of porphyrins **1** and **2** may be related to their properties (1) to internalize into cells better than **TMPyP4** or (2) to bind to G4 DNAs, which are present more abundantly in the genome of cancer cells than in normal cells.

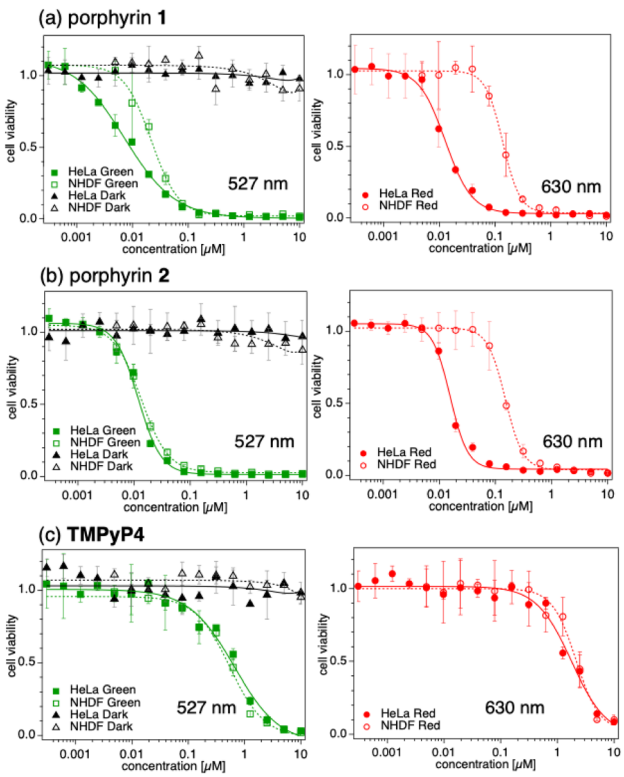

Fig. 5 Photocytotoxicities of porphyrins **1** (a), **2** (b) and **TMPyP4** (c) under the irradiation of green LEDs (max: 527 nm max, 230 mW cm^{-2} for 15 min, left column) and red LEDs (max: 630 nm, 255 mW cm^{-2} for 15 min, right column) on HeLa and NHDF cells measured by MTT assay.

Table 1 IC_{50} values of photoinduced cytotoxicity of **1**, **2**, and **TMPyP4**. Values are obtained from Hill equation fitting of the data points shown in Fig. 5 using Igor Pro 9 software

	IC_{50} (SE) [nM]			
	HeLa		NHDF	
Compounds	Green	Red	Green	Red
1	7.2 (0.6)	12.8 (0.7)	21.8 (2)	138 (5.5)
2	11.9 (0.7)	15.6 (0.7)	13.4 (0.9)	150 (4.4)
TMPyP4	657 (126)	1773 (376)	543 (67)	2130 (289)

Cellular uptake by flow cytometry and fluorescence microscopy

By taking advantage of the observation that porphyrins **1**, **2**, and **TMPyP4** are fluorescent compounds (Fig. 2), the cellular uptakes of these molecules to HeLa and NHDF were estimated by flow cytometry. The measurements were conducted with a laser excitation of 405 nm and detected with a filter of 678–706 nm based on fluorescence spectroscopy with an excitation wavelength at 405 nm, confirming that the fluorescence intensities of compounds **1**, **2**, and **TMPyP4** are similar in this detection wavelength range (Fig. S44). As a preliminary experiment, time-dependent cellular uptake of porphyrins was tested to confirm that the cellular uptake was saturated at 24 h of co-incubation.

Cells were incubated in the presence of each porphyrin (10 μM) for 24 h before being subjected to flow cytometry analyses. As shown in Fig. 6, cellular uptake of each porphyrin was observed by flow cytometry. The

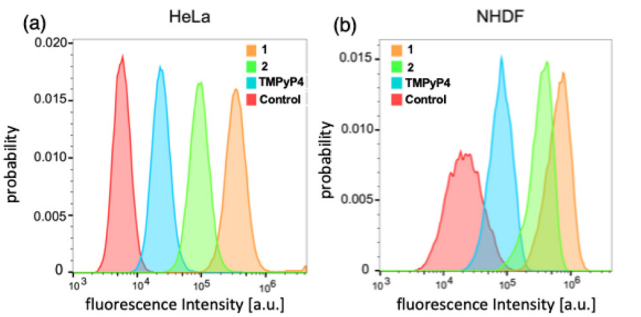

Fig. 6 Flow cytometry analyses of fluorescence emission after exposure to porphyrins **1**, **2** and **TMPyP4** (10 μM) in HeLa (a) and NHDF (b) cell lines. Cells were incubated with porphyrins for 24 h and analysed with an excitation wavelength of 405 nm and detection of emission 692 ± 14 nm. Mean values are: (a) 399 000 (porphyrin **1**), 99 500 (porphyrin **2**), 26 000 (**TMPyP4**), and 6180 (control) and (b) 670 000 (porphyrin **1**), 359 000 (porphyrin **2**), 85 200 (**TMPyP4**), and 25 700 (control).

This journal is © The Royal Society of Chemistry 2026

Open Access Article. Published on 01 October 2025. Downloaded on 6/13/2026 9:49:03 PM. This article is licensed under a Creative Commons Attribution-NonCommercial 3.0 Unported Licence.

fluorescence intensity from the cells treated with porphyrins was in the order porphyrin **1** > porphyrin **2** > **TMPyP4** in both cell lines and in line with the results from photocytotoxicity. In HeLa cells, the fluorescence intensities observed in the cells treated with **1** and **2** were, respectively, *ca.* 13 and 4 times higher than those in the cells treated with **TMPyP4**, indicating the higher cellular uptake of **1** and **2** presumably due to their larger hydrophobic cores giving more amphiphilic nature. The cells treated with compound **1** had significantly higher fluorescence intensity than **2** suggesting that guanidinium arms facilitated the uptake of the molecules, possibly in similar mechanisms to that observed in the uptake of arginine rich peptides.[48] In NHDF cells treated with porphyrins **1** and **2**, fluorescence intensity was, respectively, *ca.* 8 and 4 times higher than the one treated with **TMPyP4**. When compared between HeLa and NHDF, the mean values of fluorescence intensity observed in NHDF cells were higher than those in HeLa cells under all conditions (including control without chemicals), which is likely due to the larger size of the NHDF cells compared to HeLa cells, as can be seen in the forward scatter analysis of the flow cytometry data (Fig. S45–S52).

Cellular uptake of the porphyrins was further confirmed by fluorescence microscopy of the HeLa and NHDF cells, incubated in the presence of each porphyrin (10 μM) for 24 h. The cells were fixed and subjected to imaging using excitation (390/18 nm) and detection using a fluorescence filter of 700/75 nm. HeLa and NHDF cells treated with either compound **1** or compound **2** exhibited bright fluorescence, confirming porphyrin uptake (Fig. S53–S58).

Localization of porphyrins in permeabilized cells

It has been reported that cancer cells have more G4-forming domains in comparison to normal cells.[22,23] To explain, at least in part, the higher photocytotoxicity of porphyrins **1** and **2** observed on HeLa cells in comparison to the NHDF cells, we tried to visualize the possible binding of porphyrins **1** and **2** to G4 domains using the cells that were fixed ahead of the exposure to porphyrins. Both HeLa and NHDF cells were subjected to permeabilization with 0.5% Triton X-100 and fixed with paraformaldehyde. Subsequently, the cells were co-incubated with porphyrins **1** and **2** (5 μM) and subjected to confocal microscopy imaging.

As shown in Fig. 7, in HeLa cells, porphyrin **1** was detected both in the cytoplasm and nuclei, with some enrichment in nucleoli, while **1** was detected mostly in the cytoplasm in NHDF. In contrast, porphyrin **2** was specifically detected in the nuclei with strong enrichment in nucleoli of Hela, while **2** showed strong intensity in the cytoplasm of NHDF cells with weak signals in the nuclei of some cells. These observations may suggest that both porphyrins **1** and **2** interact with G4 DNA or G4 RNA, which may be more enriched in nuclei of cancer cells than in normal cells. Cytoplasmic signals may represent their interaction with the mitochondrial DNA or cytoplasmic RNAs.

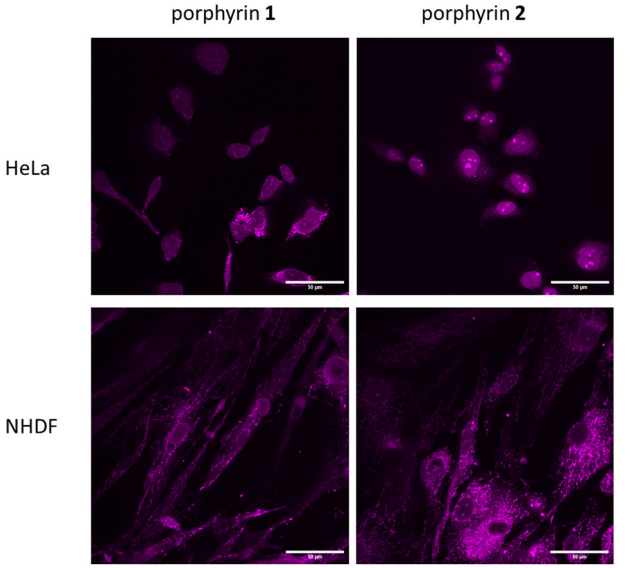

Fig. 7 Fluorescence microscopy images of HeLa cells and NHDF cells in the presence of porphyrins **1** and **2** (5 μM). Cells were permeabilized and fixed prior to the addition of porphyrins. (Excitation: 405 nm laser, emission filter: ET700/75).

Interaction of porphyrin 1 or 2 with telo24 DNA

To investigate more about the potential interaction of porphyrins and G4 DNA in cells, we investigated the G4-binding ability of **1** and **2** using G4 DNA in solution using **TMPyP4** as a standard. The possible interaction of **1** or **2** with G4 DNA was measured by fluorescence spectroscopy, FRET melting assay, UV-vis titration, and CD measurements. **TMPyP4**, a known G4-binder, was used as a standard, and the telo24 DNA (d(TTAGGG)$_4$), a human telomeric DNA sequence that **TMPyP4** binds, was used as a G4 DNA.[25]

Fluorescence spectroscopy. To a solution of each porphyrin (**1**, **2**, or **TMPyP4**, 5 μM) in pH 7.4 HEPES buffer, telo24 G4 DNA was added at 0 to 15–25 μM. In the experiments with a known G4-binder, **TMPyP4** (Fig. 8c), an increase in the emission at 660 nm was observed upon addition of telo24 in good agreement with previous reports, suggesting that some changes of the local environment of **TMPyP4** were caused by the binding to G4 DNA.[49–51] In the case of porphyrin **1**, upon addition of telo24 DNA, fluorescence intensity at 651 nm decreased dose-dependently (Fig. 8a). This could be explained by photo-induced electron transfer from the electron rich guanine to the porphyrin, similar to previous reports on the fluorescence quenching by DNA.[52,53] The fluorescence intensity of porphyrin **2** at 648 nm showed an initial decrease upon addition of lower concentrations of DNA and a subsequent increase at higher concentrations of DNA with a slight red shift (650 nm), with a somewhat similar tendency to **TMPyP4**, indicating similar interaction modes between **TMPyP4** and **2**.

FRET melting assay. Based on the fluorescence measurements above indicating the possible interaction of porphyrins **1** and **2** with telo24 G4 DNA (Fig. 8), the G4 DNA-

Open Access Article. Published on 01 October 2025. Downloaded on 6/13/2026 9:49:03 PM. This article is licensed under a Creative Commons Attribution-NonCommercial 3.0 Unported Licence.

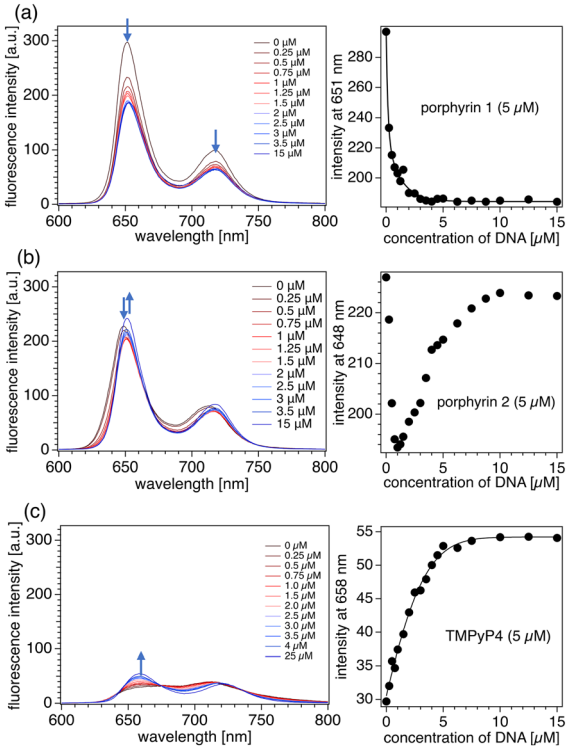

Fig. 8 Fluorescence spectra of **1** (a), **2** (b) and **TMPyP4** (c) (5 μM) in 10 mM HEPES, (pH 7.4 with 1 mM Na_2EDTA and 100 mM KCl) in the presence of telo24 G4 DNA (0–15 μM). Excitation wavelength: 423 nm for **1**, 420 nm for **2** and 432 nm for **TMPyP4**.

stabilization abilities of the porphyrins were evaluated by a FRET melting assay. To a telo24 G4 FRET probe, functionalized with 6-carboxylfluorescein (FAM) at the 5′-end and tetramethyl rhodamine (TAMRA) at the 3′-end, each porphyrin (**1**, **2**, or **TMPyP4**) was added and subjected to fluorescence intensity measurements at 510–530 nm (with a wavelength of 450–480 nm) at various temperatures. With a temperature increase from 25 to 100 °C, the FAM emission derived from destabilized G4 probes was increased corresponding to the quenching of FRET signals (Fig. S59).

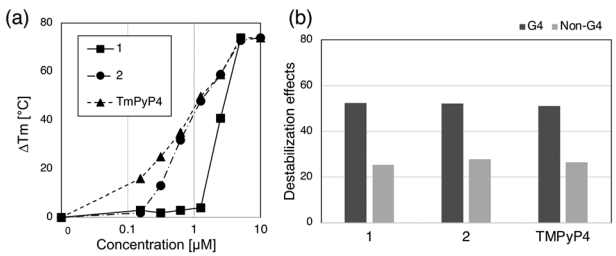

Fig. 9 (a) The stabilization of G4 DNA by porphyrins, analyzed by FRET assay. The change of T_m values (ΔT_m) of telo24 G4 DNA in the presence of the porphyrin **1**, **2** or **TMPyP4** compared to those without the compounds was plotted. (b) The selectivity for G4 DNA of porphyrins analyzed by competition FRET assay. The normalized FAM emission signals of the labeled G4 probe in the presence of competitor telo24 G4 DNA (G4) or telo24 mutant (non-G4) were shown.

In the presence of G4 stabilizers, this increase is suppressed. As shown in Fig. 9a, both porphyrins **1** and **2** showed dose-dependent stabilization effects of G4 DNA at concentrations above 1.3 and 0.16 μM, respectively. While porphyrin **1** required higher concentration to stabilize G4 DNA, G4 stabilization by **2** was more efficient than **1**, with efficiency similar to that of **TMPyP4** (Fig. 9a).

Since many G4-binders interact not only with G4 DNA but also with non-G4 DNA, the specificity of each porphyrin in stabilizing G4 over non-G4 DNA was investigated by a competitive FRET test. The non-labelled competitor, (1) telo24 G4 DNA (a G4 competitor) or (2) ssDNA with a telo24 mutant sequence (a non-G4 competitor), was added to the FRET assay system and the stabilization effect by the porphyrins was evaluated. The G4 stabilization was decreased significantly by the addition of competitor G4 DNA but not by non-G4 DNA (Fig. S60). Notably, in the presence of the G4 competitor, stronger effects of G4 destabilization were observed in comparison to the case of the non-G4 competitor (Fig. S60 and S61). At temperatures with the highest differences in destabilization between G4 and non-G4 competitors (47, 40, and 25 °C respectively for **1**, **2**, and **TMPyP4**) (Fig. S62), the destabilization effects by the competitors were quantified. As a result, in the presence of **1**, the destabilization effect of G4 and non-G4 competitors were 52% and 25%, respectively, indicating that the stabilization selectivity of **1** with G4 over non-G4 was 2.1 times larger (Fig. 9b and Table S2). Similarly, the stabilization selectivity of **2** with G4 over non-G4 was 1.9 times larger, estimated from the destabilization effect by the G4 competitor (53%) and non-G4 competitor (28%). The results for the standard compound **TMPyP4** (1.9 times) was in line with a previous report,[54] indicating that porphyrins **1** and **2** present G4 stabilization effects with selectivity for G4 DNA at a level similar to that shown by **TMPyP4**.

UV-vis titration. To obtain more insight into the interactions of porphyrins **1** and **2** with G4 DNA, we employed a UV-vis titration assay. Measurements were performed with 5 μM porphyrin solution in pH 7.4 HEPES buffer in the presence of various concentrations of telo24 DNA (0 to 15 μM) (Fig. 10). Upon addition of telo24 DNA, a significant red shift at the Soret band of the porphyrins was observed in all compounds, indicating that all three porphyrins had some interaction with telo24 DNA. As a result, compound **1** revealed a bathochromic shift of the Soret band (from 419 to 422 nm) with hypochromism upon addition of telo24 DNA (Fig. 10a). Compound **2** and **TMPyP4** showed a similar pattern with changes of the Soret band (416 nm and 422 nm), which decreased in the presence of lower concentrations (0–2 μM) of telo24 DNA and displayed an increase of new peaks (424 nm for **2** and at 437 nm for **TMPyP4**) at higher concentration (≥3 μM) (Fig. 10b and c). These results suggest that there is some difference in the binding mode of porphyrin **1** *versus* porphyrin **2** and **TMPyP4** to the telo24 DNA. Both porphyrin **2** and **TMPyP4** revealed an isosbestic point respectively at 420 and 432 nm, while

 This journal is © The Royal Society of Chemistry 2026

Open Access Article. Published on 01 October 2025. Downloaded on 6/13/2026 9:49:03 PM. This article is licensed under a Creative Commons Attribution-NonCommercial 3.0 Unported Licence.

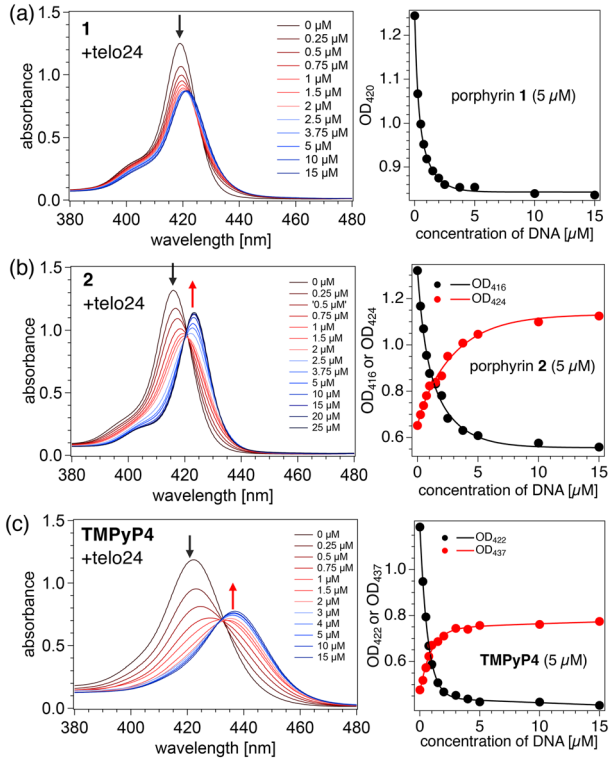

Fig. 10 UV-vis absorption spectra at around the Soret band of **1** (a), **2** (b) and **TMPyP4** (c) (5 μM) in 10 mM HEPES (pH 7.4 with 1 mM Na_2EDTA and 100 mM KCl) in the presence of telo24 G4 DNA (0–15 μM).

TMPyP4 showed a higher red shift than porphyrin **2** in the presence of telo24. The spectral pattern of **TMPyP4** with G4 DNA was in line with previous reports.[49,55]

From the UV-vis titration data, K_d values for **1**, **2** and **TMPyP4** with telo24 DNA were calculated (Fig. S63 and 64) and are listed in Table 2.[56] It was observed that **2** showed a relatively lower K_d value with slower dissociation kinetics, indicating stronger affinity towards the telo24 DNA, whereas **1** and **TMPyP4** had similar K_d values. Selectivity in the K_d values of these porphyrins to G4 DNA over dsDNA was evaluated by titration studies performed using calf thymus (CT) DNA under the same conditions (Fig. S65–S67). Calculated K_d values were much higher with CT DNA in comparison to telo24 DNA in all porphyrins. When comparing these porphyrins, higher K_d values were observed for both **1** and **2** in comparison to **TMPyP4**, indicating that the dissociation kinetics of **1** and **2** from CT DNA was much faster than **TMPyP4**, showing better G4 selectivity of **1** and **2** (Table 2).

Circular dichroism. To investigate the effect of porphyrins on the topologies of G4-forming DNA, circular dichroism (CD) measurements were employed. It has been reported that human telomeric DNA is polymorphic and observed to form several topologies.[57,58] Among them, 3 + 1 types of hybrid structures are most relevant in the presence of higher K^+ concentrations,[59] which is a similar condition to the one in the cells (*ca.* 140 mM).[60] In this study, the effect of porphyrins **1**, **2**, and **TMPyP4** on the topologies of telo24 DNA was investigated by CD studies under three conditions: (1) in the presence of 100 mM KCl, (2) in the presence of 100 mM NaCl, and (3) in the absence of K^+ and Na^+, which were supposed to provide different 3D topologies of G4. In the presence of K^+, a CD signal with a maximum at 295 nm and a minimum around 240 nm with two shoulders around 247 and 270 nm was observed for telo24 DNA (Fig. 11).[61] To this DNA, each porphyrin was added at various concentrations.

As shown in Fig. 11a, the CD signal at 295 nm increased in the presence of 6.25 μM (0.5 equiv.) of porphyrin **1**, while no additional increase was observed by further addition of **1** (≥12.5 μM). In the case of porphyrin **2**, on the other hand, an enhanced CD band of telo24 at 295 nm was observed dose-dependently up to 4–5 equivalent addition of porphyrin (Fig. 11b), with a simultaneous increase of the CD shoulder bands at 270 nm and a decrease of the shoulder at 247 nm. These results suggest that the 3 + 1 hybrid topology of telo24 DNA was more stabilized in the presence of porphyrin **2**. Under the same concentrations, the addition of the control **TMPyP4** resulted only in a slight decrease of the signal at 295 nm (Fig. 11c).

CD spectra measured in the presence of 100 mM NaCl are shown in Fig. S68. Under this condition, telo24 DNA forms an antiparallel conformation, indicated by characteristic signals at 295 nm (maximum) and at 265 nm (minimum).[58,62] Upon addition of porphyrin **1**, CD spectra of telo24 resulted in a slight decrease of the peak at 295 nm and a slight increase of the peak at 265 nm (Fig. S68a). The addition of porphyrin **2**, resulted in the signal increases at 295 nm and a decrease at 265 nm (Fig. S68b), suggesting the destabilization of telo24 in an antiparallel conformation by **2**. Addition of the control **TMPyP4** caused the decreases at both 295 nm and 265 nm signals (Fig.

Table 2 Summary of UV-vis titration data of porphyrins **1**, **2**, and **TMPyP4** with telo24. Values were obtained using linear regression on the binding model developed by Wolfe *et al.*[56] using GraphPad Prism 8 software

Compounds	λ_{max} [nm]	K_d [μM] (SE) telo24 DNA	K_d [μM] (SE) CT DNA
1	419	0.75 (0.08)	67.7 (5.6)
2	416	0.34 (0.07)	64.8 (6.2)
TMPyP4	422	0.93 (0.18)	48.1 (5.2)

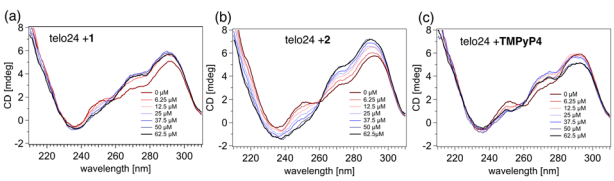

Fig. 11 CD spectra of telo24 DNA (12.5 μM) in the presence of 0–62.5 μM of porphyrin **1** (a), porphyrin **2** (b), and **TMPyP4** (c) in pH 7.4 Tris–HCl buffer (50 mM) in the presence of 100 mM KCl and 1 mM Na_2EDTA.

Open Access Article. Published on 01 October 2025. Downloaded on 6/13/2026 9:49:03 PM. This article is licensed under a Creative Commons Attribution-NonCommercial 3.0 Unported Licence.

S68c). In the absence of K^+ and Na^+, all three porphyrins cause an increase of the 295 nm peak, especially in the case of compound **2**, presumably due to its ability to induce the formation of G4 (Fig. S69).

Experimental

Detection of ROS by ESR spin trapping reagents. ESR spectra were recorded on a Bruker EMX, Continuous Wave X-Band EPR spectrometer (Bruker BioSpin GmbH, Rheinstetten, Germany). A Suprasil® ESR tube with a diameter of 4 mm, a length of 250 mm and a wall thickness of 0.8 mm was used (SP Wilmad-LabGlass, NJ, USA). 2,2,6,6-Tetramethylpiperidin-4-one (4-oxo TEMP) was purchased from ABCR (Karlsruhe, Germany) and purified by sublimation prior to use. Irradiation was performed with green (539–541 nm, 90 ± 34% lm W^{-1}) or red LED light (616–626 nm, 30 ± 37% lm W^{-1}) from Lumiflex300 Pro RGB LED Stripes (LUMITRONIX LED-Technik GmbH, Hechingen, Germany), 120 LED lamps assembled in an aluminium cylindrical container with a diameter of 8.5 cm.

DNA photocleavage assay. A mixture of an aliquot (10 μL) of DNA solution (25 ng μL^{-1} in Tris–HCl buffer) and **1**, **2** or **TMPyP4** solution in water (10 μL) with each concentration was irradiated in a U-shape 96-well (round bottom) by Lumidox® II 96-well LED array (Analytical Sales and Services, Inc., NJ, USA) equipped with either 527 nm max (230 mW cm^{-2}) or 630 nm max LEDs (255 mW cm^{-2}) for 10 min. Subsequently, gel loading dye purple (6×) (4 μL) was added to each well, and each mixture was analysed by electrophoresis (1% agarose in 0.5× TBE buffer) run at 100 V for 80 min using 0.5× TBE as the running buffer. The gel was stained using GelRed® nucleic acid stain for 1 h and subjected to a ChemiDoc Imaging System (Bio-Rad Laboratories, Inc., CA, USA). The images were analyzed using ImageJ software.

Photocytotoxicity assay. The photocytotoxicity of **1**, **2** and **TMPyP4** was tested on HeLa and NHDF cell lines. HeLa and NHDF cells were purchased from ATCC (Manassas, VA, USA). Preincubated cells were harvested at the log-growth-phase and a cell suspension in growth medium (DMEM containing 10% FBS, 2 mM glutamine, and 1% penicillin–streptomycin (100 μL)) was seeded to a 96-well plate (flat bottom) with a density of 1000 cells per well. After incubation for 24 h at 37 °C with a 5% CO_2 atmosphere, the medium of each well was exchanged with the porphyrin solutions in growth media and the cells were incubated for an additional 24 h. Subsequently, cells were washed with PBS(−) and phenol red-free DMEM was added to each well. The cells in 96-well plates were subjected to photoirradiation using a Lumidox® II 96-well LED Array with green LEDs (230 mW cm^{-2}) or red LEDs (255 mW cm^{-2}) for 15 min. After photoirradiation, the DMEM medium in each well was exchanged with MTT solution in phenol red-free DMEM (0.5 mg mL^{-1}, 100 μL) and cells were incubated for an additional 3 h. Subsequently, the medium was removed from each well and was replaced with DMSO (100 μL) to measure the OD_{560} values to evaluate cell viabilities relative to the negative control (no chemical) and positive control (treated with Tween-20).

Flow cytometry. HeLa and NHDF cells at the log-growth-phase were seeded in a 6-well plate with a density of 3×10^6 cells per well and incubated in growth medium for 24 h. Subsequently, the cells were incubated in the presence of 10 μM of each porphyrin for an additional 24 h. Cells were treated with trypsin and centrifuged and obtained pellets were washed with PBS(−)three times and resuspended in PBS(−) (500 μL) for measurement. Flow cytometry measurements were performed on a Cytek® Aurora system (Cytek Biosciences, Fermont, CA, USA). Data were analyzed using FlowJo software with the V12 channel (excitation wavelength: 405 nm; emission wavelength: 692 nm (center) with 28 nm width).

Confocal microscopy. Both HeLa and NHDF cells were incubated in Gibco™ DMEM high glucose containing 10% FBS and 1% penicillin–streptomycin. The cells at the log-growth-phase were treated with trypsin and seeded in ibidi™ μ-Slide 8 wells with a density of 10 000 cells in 250 μL. Subsequently, the cells were washed with PBS(−), fixed using a 4% paraformaldehyde solution, and permeabilized with 0.5% Triton X-100 (1 min) and exposed to porphyrins (5 μM in PBS(−)) for 5 min. Cells were washed with PBS(−) and subjected to confocal fluorescence imaging in N_2-saturated PBS(−) on a microscope (Nikon TiE2) with a Yokogawa Confocal Scanner Unit CSU-W1 (excitation: 405 nm laser, emission filter: ET700/75).

Fluorescence spectroscopy. Fluorescence emission spectra were recorded on a Varian Cary Eclipse spectrophotometer (Agilent Technologies, Inc., Santa Clara, California, U.S.). Each solution of **1**, **2** or **TMPyP4** (5 μM) was prepared in 10 mM HEPES buffer (pH 7.4, containing 100 mM KCl and 1 mM Na_2EDTA). A solution of single strand telo24 DNA (500 μM) with the sequence of *d*(TTAGGGTTAGGGTTAGGGTTAGG G) was prepared in the same buffer and subjected to the pre-annealing process by heating at 90 °C for 10 min and cooling back to room temperature over 3 h. To each porphyrin solution (2 mL) in a quartz cuvette (path length: 1 cm), an aliquot of the DNA solution was added and left to equilibrate for 2 min upon mixing to record the fluorescence spectra.

FRET melting assay. G4 stabilization by porphyrins was tested by FRET assay using telo24 DNA labelled with 6-carboxyfluorescein (FAM) at the 5″-end and tetramethyl-rhodamine (TAMRA) at the 3′-end (Fasmac Co., Ltd., Kanagawa, Japan). The details are described in the SI.

UV-vis. UV absorption spectra were recorded on a JASCO V-570 UV/vis/NIR spectrophotometer (JASCO Co., Tokyo Japan). Each solution of **1**, **2** or **TMPyP4** (5 μM) was prepared in 10 mM HEPES buffer (pH 7.4, containing 100 mM KCl and 1 mM Na_2EDTA). A solution of single strand telo24 DNA (500 μM) with the sequence of *d*(TTAGGGTTAGGGTTAGGGTTAGG G) was prepared in the same buffer and subjected to the pre-annealing process by heating at 90 °C for 10 min and cooling back to room temperature over 3 h. To each porphyrin solution (2 mL) in a quartz UV cuvette (path length: 1 cm), an

 This journal is © The Royal Society of Chemistry 2026

Open Access Article. Published on 01 October 2025. Downloaded on 6/13/2026 9:49:03 PM. This article is licensed under a Creative Commons Attribution-NonCommercial 3.0 Unported Licence.

aliquot of the DNA solution was added and left to equilibrate for 2 min upon mixing to record the UV-vis spectra. The titration was stopped when there was no change observed upon addition of DNA.

Circular dichroism. CD spectra were recorded on a Jasco J-1500 circular dichroism spectrophotometer (JASCO Co., Tokyo Japan). A high performance quartz cell with an optical path of 1 mm was used. Solutions of telo24 DNA (12.5 μM) in 10 mM Tris–HCl buffer (pH 7.4) were prepared under three different conditions: containing (1) 100 mM KCl, (2) 100 mM NaCl or (3) without K^+ or Na^+. To the DNA solution in each buffer, an aliquot of compound **1**, **2** or **TMPyP4** was added to measure the CD spectrum.

Conclusions

Two types of cationic porphyrin derivatives, **1** and **2**, were designed and synthesized as bi-functional molecules with photosensitization and G4 DNA-binding activity. In comparison to a well-studied standard G4 binder **TMPyP4**, **1** and **2** exhibited similar $^1O_2$ generation and dsDNA cleavage. However, significantly enhanced photocytotoxicity was observed in **1** and **2** compared to **TMPyP4**, presumably due to better cellular internalization of the molecules. Interactions with telo24 G4 DNA were studied by spectroscopic methods, revealing similar levels of binding stability and slightly better selectivity with **1** and **2** compared to **TMPyP4**. Interestingly, stronger photocytotoxicity was observed in a cancer cell line (HeLa) in comparison to the normal cells (NHDF) with all porphyrins (**1**, **2**, and **TMPyP4**) upon red light irradiation. This may be related to more abundant existence of G4 on the cancer cell genomes. This is in line with the localization of porphyrin molecules in cellular nuclei observed by fluorescence microscopy. Recently, we reported bifunctional Gd(III)- and Mn(III)-porphyrin molecules with photosensitization and relaxivity.[63,64] Considering the excellent photosensitivity of porphyrins **1** and **2** in this study, with binding ability to human telomeric G4, these molecules can be considered as promising model compounds for further development as G4 targeting photosensitizers.

Author contributions

N. Y.-S., H. M., and Y. Y. designed the overall project. C. C. designed detailed structures of the molecules and contributed to their synthesis and structural characterization in collaboration with Y. Y. N. K. performed FRET assay in collaboration with H. M. and N. Y.-S. C. C. performed fluorescence, UV-vis, and CD spectroscopy. C. C. performed ROS generation assay by ESR, DNA cleavage tests, photocytotoxicity assay, and fluorescence microscopy analyses in collaboration with S. S. L. and Y. Y. T. X. performed flow cytometry assay in collaboration with C. C. and Y. Y. The manuscript was written with contributions of all authors. All authors have given approval to the final version of the manuscript.

Conflicts of interest

There are no conflicts to declare.

Data availability

Supplementary information: experimental data and details regarding the synthesis, ESR, UV-vis, fluorescence and flow cytometry; DNA photocleavage, photocytotoxicity assays; fluorescence and confocal microscopy images are available in the supplementary information (SI). See DOI: **https://doi.org/10.1039/D5MD00706B**.

The data supporting this article have been included as part of the SI.

Acknowledgements

The authors thank Ms. Staudhammer in the D-CHAB at ETH for their help in correcting the manuscript. The authors thank Dr. Ebert in ETH for his support in ESR measurements. The authors thank Prof. Leroux in ETH for his support in fluorescence measurements. The authors thank Prof. Bode in ETH for his support in CD and UV-vis measurements. ScopeM of ETH, MoBiAS and the NMR service in the D-CHAB at ETH are acknowledged for their help in the measurements.

This research was supported by SNF Strategic Japanese-Swiss Science and Technology Program (IZLJZ2_183660, Y. Y.), JSPS under the Joint Research Program implemented in association with SNF (20191508, H. M. and N. Y.-S.), SNF Project Funding (205321_173018, Y. Y.), ETH Research Grants (ETH-21_15-2; ETH-36_20-2), and JSPS KAKENHI (Grant-in-Aid for Scientific Research [A], 6251004, H. M.; Grants-in-Aid for Scientific Research on Innovative Areas, 21H00264, 22H04707, H. M.; Grant-in-Aid for Scientific Research [C], 15K07164, N. Y.-S.).

Notes and references

1 J. F. Lovell, T. W. B. Liu, J. Chen and G. Zheng, *Chem. Rev.*, 2010, **110**, 2839–2857.
2 R. K. Pandey and G. Zheng, *The Porphyrin Handbook*, 2000, vol. 6, pp. 157–230.
3 S. Nakajima, H. Hayashi, Y. Omote, Y. Yamazaki, S. Hirata, T. Maeda, Y. Kubo, T. Takemura, Y. Kakiuchi, Y. Shindo, K. Koshimizu and I. Sakata, *J. Photochem. Photobiol., B*, 1990, **7**, 189–198.
4 K. W. Woodburn, S. Stylli, J. S. Hill, A. H. Kaye, J. A. Reiss and D. R. Phillips, *Br. J. Cancer*, 1992, **65**, 321–328.
5 K. Hiyama, H. Matsui, M. Tamura, O. Shimokawa, M. Hiyama, T. Kaneko, Y. Nagano, I. Hyodo, J. Tanaka, Y. Miwa, T. Ogawa, T. Nakanishi and I. Tamai, *J. Porphyrins Phthalocyanines*, 2013, **17**, 36–43.
6 T. Tojo, K. Nishida, T. Kondo and M. Yuasa, *Bioorg. Med. Chem. Lett.*, 2020, **30**, 127437.
7 K. Nishida, T. Tojo, T. Kondo and M. Yuasa, *Sci. Rep.*, 2021, **11**, 2046.
8 R. Wang, X. Li and J. Yoon, *ACS Appl. Mater. Interfaces*, 2021, **13**, 19543–19571.

Open Access Article. Published on 01 October 2025. Downloaded on 6/13/2026 9:49:03 PM. This article is licensed under a Creative Commons Attribution-NonCommercial 3.0 Unported Licence.

9 A. B. Mihoub, L. Larue, A. Moussaron, Z. Youssef, L. Colombeau, F. Baros, C. Frochot, R. Vanderesse and S. Acherar, *Molecules*, 2018, **23**(8), 1936.
10 M. Tassinari, S. N. Richter and P. Gandellini, *Nucleic Acids Res.*, 2021, **49**, 3617–3633.
11 N. Kosiol, S. Juranek, P. Brossart, A. Heine and K. Paeschke, *Mol. Cancer*, 2021, **20**, 40.
12 J. Carvalho, J. L. Mergny, G. F. Salgado, J. A. Queiroz and C. Cruz, *Trends Mol. Med.*, 2020, **26**, 848–861.
13 H. Masai and T. Tanaka, *Biochem. Biophys. Res. Commun.*, 2020, **531**, 25–38.
14 S. Neidle, *FEBS J.*, 2010, **277**, 1118–1125.
15 H. Han and L. H. Hurley, *Trends Pharmacol. Sci.*, 2000, **21**, 136–142.
16 J. L. Huppert and S. Balasubramanian, *Nucleic Acids Res.*, 2007, **35**, 406–413.
17 T.-M. Ou, Y.-J. Lu, C. Zhang, Z.-S. Huang, X.-D. Wang, J.-H. Tan, Y. Chen, D.-L. Ma, K.-Y. Wong, J. C.-O. Tang, A. S.-C. Chan and L.-Q. Gu, *J. Med. Chem.*, 2007, **50**, 1465–1474.
18 D. Gomez, J.-L. Mergny and J.-F. Riou, *Cancer Res.*, 2002, **62**, 3365–3368.
19 E. Izbicka, R. T. Wheelhouse, E. Raymond, K. K. Davidson, R. A. Lawrence, D. Y. Sun, B. E. Windle, L. H. Hurley and D. D. Von Hoff, *Cancer Res.*, 1999, **59**, 639–644.
20 V. Caprio, B. Guyen, Y. Opoku-Boahen, J. Mann, S. M. Gowan, L. M. Kelland, M. A. Read and S. Neidle, *Bioorg. Med. Chem. Lett.*, 2000, **10**, 2063–2066.
21 I. M. Dixon, F. Lopez, J.-P. Estève, A. M. Tejera, M. A. Blasco, G. Pratviel and B. Meunier, *ChemBioChem*, 2005, **6**, 123–132.
22 R. Hänsel-Hertsch, D. Beraldi, S. V. Lensing, G. Marsico, K. Zyner, A. Parry, M. Di Antonio, J. Pike, H. Kimura, M. Narita, D. Tannahill and S. Balasubramanian, *Nat. Genet.*, 2016, **48**, 1267–1272.
23 K.-W. Zheng, J.-Y. Zhang, Y.-D. He, J.-Y. Gong, C.-J. Wen, J.-N. Chen, Y.-H. Hao, Y. Zhao and Z. Tan, *Nucleic Acids Res.*, 2020, **48**, 11706–11720.
24 Q. F. Yang, X. R. Wang, Y. H. Wang, X. H. Wu, R. Y. Shi, Y. X. Wang, H. N. Zhu, S. Yang, Y. L. Tang and F. Li, *Nucleic Acids Res.*, 2024, **53**, D91–D98.
25 R. T. Wheelhouse, D. Sun, H. Han, F. X. Han and L. H. Hurley, *J. Am. Chem. Soc.*, 1998, **120**, 3261–3262.
26 L.-N. Zhu, S. Shi, L. Yang, M. Zhang, K.-K. Liu and L.-N. Zhang, *RSC Adv.*, 2016, **6**, 13080–13087.
27 P. Zhao, M.-C. Liu, M. Zheng, S.-F. Jin, D.-T. Tang, J. Chen, Y.-N. Ma, J.-Q. Lin, X.-H. Wang and H.-J. Liu, *Dyes Pigm.*, 2016, **128**, 41–48.
28 W. Zhou, Y. Cheng, B. Song, J. Hao, W. Miao, G. Jia and C. Li, *Biochemistry*, 2021, **60**, 3707–3713.
29 S. Wu, L. Jiang, L. Lei, C. Fu, J. Huang, Y. Hu, Y. Dong, J. Chen and Q. Zeng, *Cell Death Dis.*, 2023, **14**, 1–16.
30 E. Cadoni, L. De Paepe, G. Colpaert, R. Tack, D. Waegeman, A. Manicardi and A. Madder, *Nucleic Acids Res.*, 2023, **51**, 4112–4125.
31 M. Deiana, J. M. Andrés Castán, P. Josse, A. Kahsay, D. P. Sánchez, K. Morice, N. Gillet, R. Ravindranath, A. K. Patel, P. Sengupta, I. Obi, E. Rodriguez-Marquez, L. Khrouz, E. Dumont, L. A. Galán, M. Allain, B. Walker, H. S. Ahn, O. Maury, P. Blanchard, T. Le Bahers, D. Öhlund, J. von Hofsten, C. Monnereau, C. Cabanetos and N. Sabouri, *Nucleic Acids Res.*, 2023, **51**, 6264–6285.
32 W. Chen, Y. Zhang, H.-B. Yi, F. Wang, X. Chu and J.-H. Jiang, *Angew. Chem.*, 2023, **135**, e202300162.
33 X. Zhang, J. Wang and M.-H. Hu, *ACS Pharmacol. Transl. Sci.*, 2024, **7**, 2174–2184.
34 T. L. Ruan, S. J. Davis, B. M. Powell, C. P. Harbeck, J. Habdas, P. Habdas and L. A. Yatsunyk, *Biochimie*, 2017, **132**, 121–130.
35 J. Ren and J. B. Chaires, *Biochemistry*, 1999, **38**, 16067–16075.
36 V. Rapozzi, S. Zorzet, M. Zacchigna, E. Della Pietra, S. Cogoi and L. E. Xodo, *Mol. Cancer*, 2014, **13**, 75.
37 I. M. Dixon, F. Lopez, A. M. Tejera, J.-P. Estève, M. A. Blasco, G. Pratviel and B. Meunier, *J. Am. Chem. Soc.*, 2007, **129**, 1502–1503.
38 J. Alzeer, B. R. Vummidi, P. J. C. Roth and N. W. Luedtke, *Angew. Chem., Int. Ed.*, 2009, **48**, 9362–9365.
39 A. Membrino, M. Paramasivam, S. Cogoi, J. Alzeer, N. W. Luedtke and L. E. Xodo, *Chem. Commun.*, 2010, **46**, 625–627.
40 L. Sabater, M.-L. Nicolau-Travers, A. De Rache, E. Prado, J. Dejeu, O. Bombarde, J. Lacroix, P. Calsou, E. Defrancq, J.-L. Mergny, D. Gomez and G. Pratviel, *J. Biol. Inorg. Chem.*, 2015, **20**, 729–738.
41 L. Lecarme, E. Prado, A. De Rache, M.-L. Nicolau-Travers, G. Gellon, J. Dejeu, T. Lavergne, H. Jamet, D. Gomez, J.-L. Mergny, E. Defrancq, O. Jarjayes and F. Thomas, *ChemMedChem*, 2016, **11**, 1133–1136.
42 Porphyrin **1** is a new compound while porphyrin **2** was previously reported for photoinactivation of bacteria.
43 C. S. Prasanth, S. C. Karunakaran, A. K. Paul, V. Kussovski, V. Mantareva, D. Ramaiah, L. Selvaraj, I. Angelov, L. Avramov, K. Nandakumar and N. Subhash, *Photochem. Photobiol.*, 2014, **90**, 628–640.
44 J. S. Lindsey, I. C. Schreiman, H. C. Hsu, P. C. Kearney and A. M. Marguerettaz, *J. Org. Chem.*, 1987, **52**, 827–836.
45 J. Maillard, K. Klehs, C. Rumble, E. Vauthey, M. Heilemann and A. Fürstenberg, *Chem. Sci.*, 2021, **12**, 1352–1362.
46 Y. Lion, M. Delmelle and A. Vandevorst, *Nature*, 1976, **263**, 442–443.
47 J. Berlanda, T. Kiesslich, V. Engelhardt, B. Krammer and K. Plaetzer, *J. Photochem. Photobiol., B*, 2010, **100**, 173–180.
48 R. Brock, *Bioconjugate Chem.*, 2014, **25**, 863–868.
49 C. Wei, G. Jia, J. Yuan, Z. Feng and C. Li, *Biochemistry*, 2006, **45**, 6681–6691.
50 G. Jia, Z. Feng, C. Wei, J. Zhou, X. Wang and C. Li, *J. Phys. Chem. B*, 2009, **113**, 16237–16245.
51 C. Wei, L. Wang, G. Jia, J. Zhou, G. Han and C. Li, *Biophys. Chem.*, 2009, **143**, 79–84.
52 T. Heinlein, J.-P. Knemeyer, O. Piestert and M. Sauer, *J. Phys. Chem. B*, 2003, **107**, 7957–7964.
53 B. R. Vummidi, J. Alzeer and N. W. Luedtke, *ChemBioChem*, 2013, **14**, 540–558.

 This journal is © The Royal Society of Chemistry 2026

Open Access Article. Published on 01 October 2025. Downloaded on 6/13/2026 9:49:03 PM.
This article is licensed under a Creative Commons Attribution-NonCommercial 3.0 Unported Licence.

54 N. V. Anantha, M. Azam and R. D. Sheardy, *Biochemistry*, 1998, **37**, 2709–2714.
55 M. W. Freyer, R. Buscaglia, K. Kaplan, D. Cashman, L. H. Hurley and E. A. Lewis, *Biophys. J.*, 2007, **92**, 2007–2015.
56 A. Wolfe, G. H. Shimer and T. Meehan, *Biochemistry*, 1987, **26**, 6392–6396.
57 J. Dai, M. Carver and D. Yang, *Biochimie*, 2008, **90**, 1172–1183.
58 J. Kypr, I. Kejnovska, D. Renciuk and M. Vorlickova, *Nucleic Acids Res.*, 2009, **37**, 1713–1725.
59 A. T. Phan, *FEBS J.*, 2010, **277**, 1107–1117.
60 A. Ambrus, D. Chen, J. Dai, T. Bialis, R. A. Jones and D. Yang, *Nucleic Acids Res.*, 2006, **34**, 2723–2735.
61 R. Villar-Guerra, J. O. Trent and J. B. Chaires, *Angew. Chem.*, 2018, **130**, 7289–7293.
62 Y. Wang and D. J. Patel, *Structure*, 1993, **1**, 263–282.
63 T. Nemeth, N. Yoshizawa-Sugata, A. Pallier, Y. Tajima, Y. Ma, É. Tóth, H. Masai and Y. Yamakoshi, *Chem. Biomed. Imaging*, 2023, **1**, 157–167.
64 T. Nemeth, A. Pallier, Ç. Çelik, Z. Garda, N. Yoshizawa-Sugata, H. Masai, É. Tóth and Y. Yamakoshi, *Chem. Biomed. Imaging*, 2025, **3**, 5–14.